FISEVIER

Contents lists available at ScienceDirect

Chemical Engineering Journal

journal homepage: www.elsevier.com/locate/cej





Gecko inspired reversible adhesion via quantum dots enabled photo-detachment

Yuanyuan Mi ^{a,1}, Yingchun Niu ^{a,1}, Huiqin Ni ^a, Yida Zhang ^a, Lulu Wang ^a, Yinping Liu ^a, Melvin A. Ramos ^b, Travis Shihao Hu ^b, Quan Xu ^{a,*}

a State Key Laboratory of Heavy Oil Processing Beijing Key Laboratory of Biogas Upgrading Utilization, China University of Petroleum-Beijing, Beijing 102249, China

ARTICLE INFO

Keywords: Gecko Photothermal Remote control MoO_{3-x} quantum dots Adhesion mechanism

ABSTRACT

Inspired by the detachment behavior of gecko toe valgus, a reversible dry adhesive surface was developed, which is composed of polydimethylsiloxane (PDMS) micropillar arrays and MoO_{3-x} quantum dots (MoO_{3-x} QDs). The reversibility of adhesion is caused by the thermal expansion of the overall structure of the PDMS micropillar array due to the thermal response of MoO_{3-x} QDs to external stimuli. Under infrared laser irradiation, the interface temperature of MoO_{3-x} PDMS surface increased from 20 °C to 88.5 °C in 60 s. The MoO_{3-x} QDs-induced photothermal conversion facilitate the reduction of the real contact fraction between the bio-inspired micropillar arrays and the opposing/target surface, resulting in a significant decrease in adhesion. This work demonstrates a new strategy for realizing remote control of smart adhesives or surfaces. The mechanism elucidated in this work may find a broad application, such as in climbing robots, micro-manipulation/micro-selection in advanced manufacturing, active self-cleaning surface for solar panels, fibrillar dry adhesives and touch sensitive grippers in outer space explorations, and more.

1. Introduction

Scientists have never stopped drawing inspiration from nature for all kinds of engineering, biomedical, energy and informatics applications [1]. Since the nanoscience and nanotechnology boost in the 1990s, gecko lizards' formidable climbing and locomotor ability had been brought to light again by a landmark paper published in Nature in 2000 [2], and this interdisciplinary field rejuvenated. One of the astonishing facts is the easy-detachability or easy-release mechanism in gecko dry adhesive structures given how strong and stable the adhesion can be in the engaging state. Previous studies, including our own [3], indicate the natural digital hyperextension (DH) of gecko toes was a key factor to achieve easy and rapid detachment, and active self-cleaning. The traditional adhesive material (e.g., superglue or pressure sensitive adhesives [PSAs]) requires significant amount of energy to be removed from the attached substrate, which makes the detachment process difficult and the adhesives nonreusable [4,5]. Hence, gecko gait characteristics and the special toepad structures offer an ideal biomimetic inspiration for developing a smart dry adhesive system with integrated

functionalities, active adjustability, and fast-switching capability [6].

The reversible adhesive developed by imitating the climbing of geckos have been widely reported [7–10]. Most of these adhesives were controlled via the external stimuli-responsive, utilizing a variety of mechanisms such as magnetic fields [11–14], electric fields [15–17], temperature change [18,19], and light irradiation [20-23]. Mareike Frensemeier et al. proposed a switchable dry adhesive based on a nickeltitanium (NiTi) shape-memory alloy with an adhesive silicone rubber surface. The adhesive performance of this hybrid system is affected by the temperature-induced topographical change of the NiTi [19]. Aránzazu del Campo et al. developed arrays of PDMS micropillars containing NdFeB microparticles. The nano/micropillars undergo large bending in response to the magnetic field gradient [24]. Additionally, wang et al. fabricated a light-controlled adhesive composed (BGPP) of the PDMS/graphene composite as the backing layer and PDMS as the micropillar array. The BGPP exhibited superior adhesion under UV irradiation, which is 2.4 times greater than that of the UV-off state [23]. Despite many responsive and reversible adhesive surfaces have been developed, most of them are composed of hybrid micropillars/substrate

E-mail address: xuquan@cup.edu.cn (Q. Xu).

b Department of Mechanical Engineering, California State University, Los Angeles, CA 90032, USA

^{*} Corresponding author.

¹ Those authors contribute equally to this work

materials and structures, or rely on reinforcement concentration gradients inside the micropillars to achieve responsive control. These methods require extra steps to build a rather complex composite structure using difficult preparation process. There are a few researches on developing smart adhesives controlled by near-infrared (NIR) light signals. And it is still elusive how the photothermal effect affects morphological changes and in turn the controllability.

The present work takes inspiration from both the gecko digital hyperextension (DH) and the external stimuli responsive mechanism exited in many biological and synthetic material systems [3]. The structure of the micropillar array were controlled via light signals to simulate the gecko toe scrolling and peeling motion, enabling a switch between on and off states. Molybdenum has a rich valence state and can form a variety of molybdenum oxides (MoO_x, $1 < x \le 3$), with various shapes and structures, and is a highly efficient and stable photothermal conversion material [25]. Herein, we fabricated near-infrared responsive MoO_{3-x} QDs with excellent photothermal properties. We introduced the high-performance MoO_{3-x} QDs as fillers into PDMS pillar arrays to synthesize a new type of reversible dry adhesive. (Fig. 1) The results showed that under the irradiation of 808 nm near-infrared laser, MoO_{3,v} ODs generate heat distribution inside the PDMS and a temperature gradient, which causes the adhesive micropillars to expand nonuniformly and the adhesive patch curled up. This morphological change reduces the contact area of the adhesive with the substrate via a self-peeling process, resulting in reduced adhesion and separation from the substrate. This new kind of bionic surface is simple and easy to control. The external stimulus can be generated by remote laser, which can make the smart adhesive fall off spontaneously and avoid accidental tear. The mechanism proposed in this work stimulates more improvements in the study of self-cleaning surfaces and controllable adhesion for the stable and safe operation in extreme environments. This controllable surface is applicable in many engineering fields, such as climbing robots [26], space bonding devices, self-cleaning surfaces, and advanced grasping technologies, just to name a few.

2. Results and discussion

2.1. Fabrication of the MoO_{3-x} QDs and characterization

The synthesis route to produce the MoO_{3-x} QDs is illustrated in Fig. 2a. Firstly, the MoS_2 powder was added into 30% H_2O_2 solution to form a reaction system solution. Subsequently, the solution was transferred to an autoclave at 60 °C and CO_2 was introduced into the autoclave until the pressure reaches 40 MPa. With the presence of CO_2 , the

MoO₃ sheets can further reduce to the MoO₃ QDs. Finally, the MoO₃ QDs solution was exposed to sunlight for 3 h to form MoO_{3-x} QDs solution. The transmission electron microscopy (TEM) images (Fig. 2b) show that the as-prepared sample consists of uniformly distributed MoO_{3-x} QDs. The average lateral size was found to be about 4 nm. The high-resolution TEM images (HRTEM, Fig. 2c) further confirm the high crystalline of the MoO_{3-x} QDs, revealing a lattice spacing of about 0.34 nm. The atomicresolution high-angle annular dark-field scanning transmission electron microscopy (HAADF-STEM) image and the atomic-resolution energy-dispersive X-ray (EDX) elements mapping is shown in Fig. S2. Mo and O elements are homogeneously and evenly distributed in MoO_{3-x} QDs. In addition, we further investigated the chemical composition and structure of the MoO_{3-x} QDs. The Raman spectra of MoO_{3-x} QDs is shown in Fig. S3. The peak at 655 cm^{-1} , 813 cm^{-1} , 985 cm^{-1} is assigned to the Mo₃-O, Mo₂-O, and Mo⁶⁺=O stretching mode, respectively. All three peaks (655, 813, 985 cm⁻¹) in the Raman spectra are assigned to the MoO_{3-x} QDs. Fig. S4 is the survey binding energy measured by X-ray photoelectron spectroscopy (XPS). From the survey binding energy, the main three peaks are represented as O 1 s, C 1 s and Mo 3d. Highresolution Mo 3d peaks in Fig. 2d shows that the peaks at 231.2 eV and 234.3 eV are attributed to the $3d_{3/2}$ and the $3d_{5/2}$ orbital electrons of Mo⁵⁺. While the peaks at 233.1 eV and 236.1 eV are attributed to the bending energies of the $3d_{3/2}$ and the $3d_{5/2}$ orbital electrons of Mo⁶⁺. The appearance of Mo⁵⁺ plays an essential role in the generation of plasmon resonance. To investigate the electronic state of Mo species in MoO_{3-x} QDs, X-ray absorption near-edge structure (XANES) and extended X-ray absorption fine structure (EXAFS) were conducted. As demonstrated in the Mo K-edge XANES spectra (Fig. 2e), the Mo foil shows the minimum absorption edge energy. Meanwhile, the enlarged Mo K-edge XANES curves (inset, Fig. 2e) illustrate that the near-edge absorption energy of MoO_{3-x} QDs located between Mo foil and MoO₃, suggesting the valence state of Mo in MoO_{3-x} QDs is lower than MoO₃. This also proves that the coordination of O is less than three. The the phase and crystalline nature of the MoO_{3-x} QDs were further explored by X-ray diffraction (XRD) analysis, which is closer to the reduced species of MoO_{2.8}. (Fig. S5) Furthermore, we studied weighted calculations (Fig. S6) and the corresponding R-space curves (Fig. 2f) after a k_2 $[\chi(k)]$ weighted Fourier transform based on Mo EXAFS spectra. As shown in Fig. 2f, the shoulder peaks at around 1.5 Å and 3.1 Å in the MoO_{3-x} QDs are classed as Mo-O and Mo-Mo vectors, respectively. The electronic properties of MoO₃ QDs and MoO_{3-x} QDs were explored by the DFT calculation. The optimized structures of MoO_3 QDs and MoO_{3-x} QDs are shown as Fig. S7 and Fig. 2g. The density of state (DOS) of these two structures are compared and shown as Fig. 2h. For MoO₃ QDs, it shows a

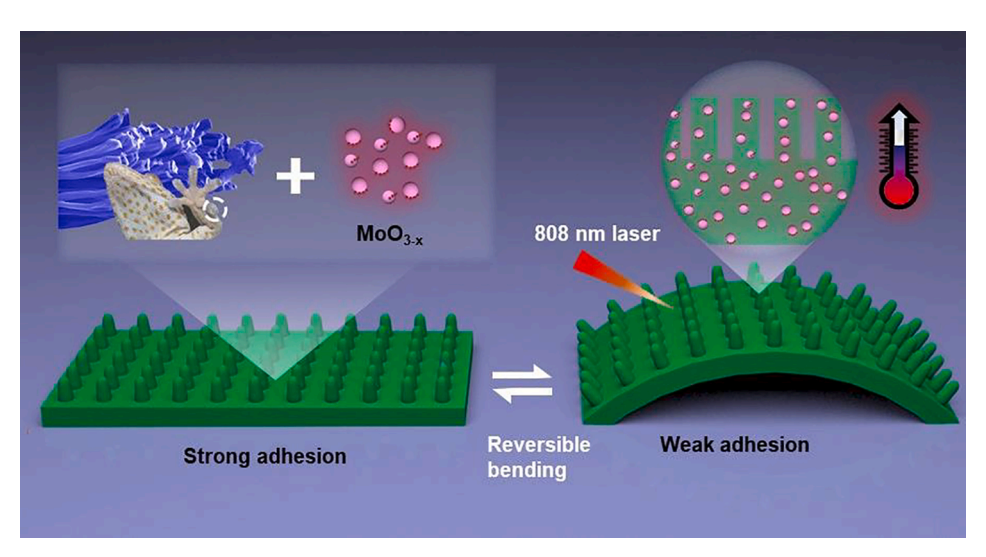


Fig. 1. Design principle and mechanism of the photothermal-introduced switchable adhesive surface.

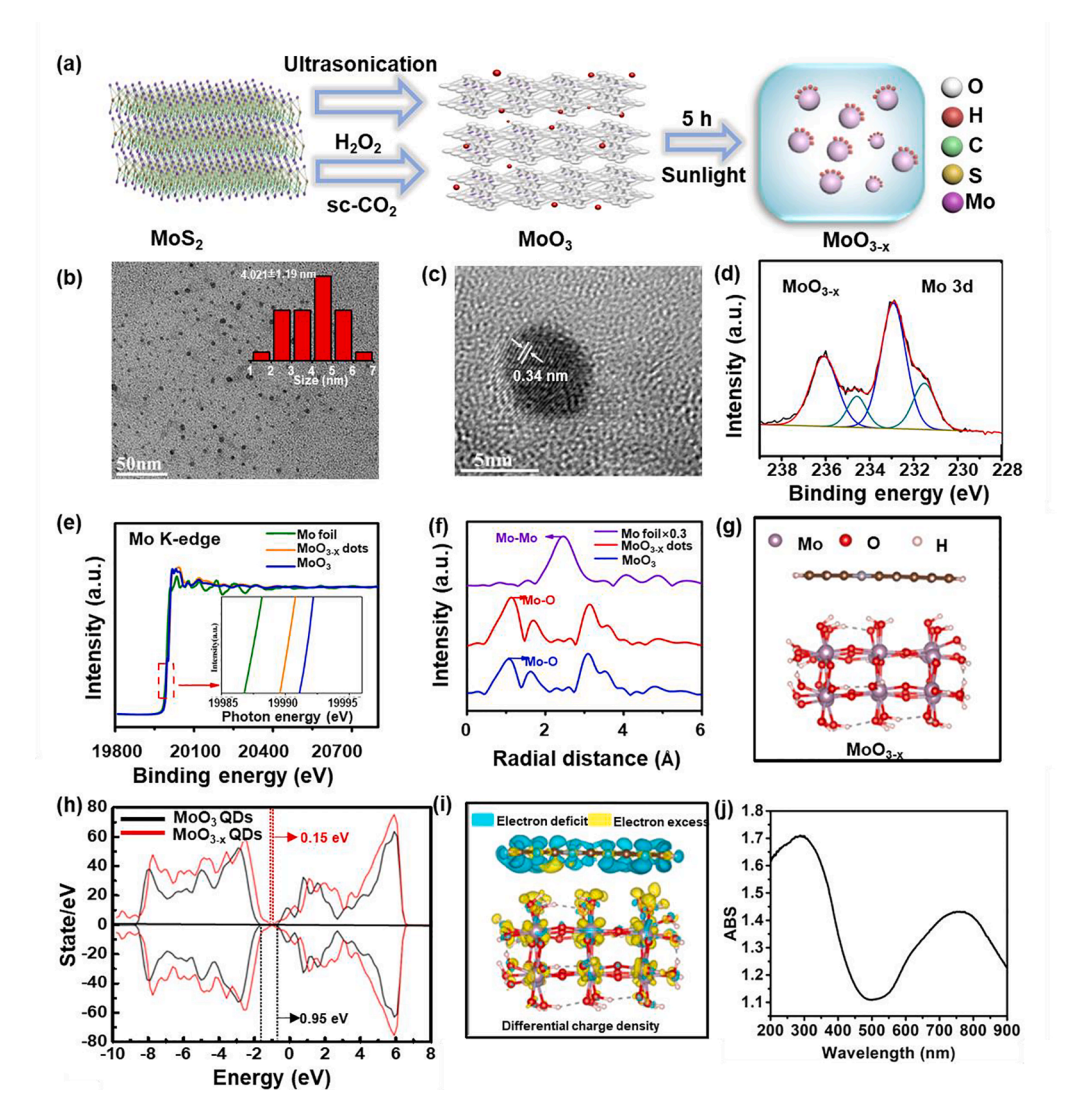


Fig. 2. (a) Schematic of the fabrication process for obtaining the MoO_{3-x} QDs. (b) TEM image of the MoO_{3-x} QDs. (c) HRTEM image of the MoO_{3-x} QDs. (d) Mo 3d core level peak regions for MoO₃. x QDs; (e) Mo K-edge X-ray absorption near-edge spectra (XANES) of MoO3-x QDs along with Mo foil and MoO3 as references; (f) Fourier-transform EXAFS spectrum of Mo foil, MoO3-x QDs and MoO3; (g) The optimized structure for MoO_{3-x} QDs. (h) Density of states (DOS) of MoO3 QDs (black line) and MoO3-x QDs (red line). (i) Electron density difference of MoO_{3-x} QDs. (j) UV-Vis-NIR absorption spectra of MoO_{3-x} QDs.

band gap of about 0.95 eV near the Fermi level. For the MoO_{3-x} QDs, the band gap reduces to 0.15 eV. The decrease of the band gap of the MoO_{3-x} QDs compared with MoO_3 correspond to the red shift of the absorption wavelength for the composite structure in the experiment. The charge difference of the composite structure is shown in Fig. 2i. The charge transfers from the carbon dot to MoO_3 . The composite structure is favorable to the electron transfer and makes the adsorption wavelength red shift. As shown in Fig. 2j the powder sample of the MoO_{3-x} QDs exhibits high optical absorbance in the whole biological window of 600-900 nm, which is due to the free electron induced Localized Surface Plasmon Resonance (LSPR) effect [27,28]. Thus, the MoO_{3-x} QDs, which could adsorb ultra-red spectrum with lower energy to generate excellent photothermal property, were successfully prepared.

2.2. The photothermal property of the bioinspired adhesive surfaces.

By introducing the MoO_{3-x} QDs into the PDMS matrix, the resultant micropillar arrays exhibit excellent photothermal property. The fabrication process of the MoO_{3-x} -PDMS adhesive is shown in Fig. 3a. First, the prepared MoO_{3-x} -PDMS solution was poured onto the silicon template of the negative geometry (vertical/straight micropores) and cast into the micropillar arrays. By carefully releasing the sample from the silicon template after curing, a bioinspired surface featuring with an array of micropillars is obtained. Fig. 3b shows the SEM images of the geometry and detentions of the MoO_{3-x} -PDMS adhesive surface at

different scales and viewing angles. The surface is composed of evenly distributed vertical micropillars with a diameter of about 5 µm and a height of about 10 µm. As shown in the energy-dispersive X-ray spectroscopy (EDX) results of MoO_{3-x}-PDMS samples, molybdenum can be observed on the surface. Meanwhile, compared PDMS micropillar array without MoO_{3-x} QDs, the distribution of molybdenum in each micropillar on the PDMS-MoO_{3-x} micropillar can be clearly seen (Fig.S8), indicating the successful doping of MoO_{3-x}-PDMS, which is another evidence MoO_{3-x} QDs are uniformly distributed. In order to investigate different factors of MoO_{3-x} QDs on the photothermal effects, we have first studied the effect of NIR irradiation on pure MoO_{3-x} solution of different concentrations. As shown in Fig. 3c, after 10 min of irradiation by an 808 nm laser, the temperature was increased from 25 °C to 55 °C, 50 °C, 45 °C for 500, 200, 100 μ g/mL MoO_{3-x} solution, respectively. Hence the increased temperature was due to the increase of the MoO_{3-x} concentration in the solutions under the same time of 808 nm laser irradiation. The temperature changes of the 500 $\mu g/mL$ MoO_{3-x} solution were consistent in five cycles tested, showing excellent photothermal stability (Fig. S11). The results indicated not only that MoO_{3-x} QDs possessed a good photothermal effect, but more importantly the MoO_{3-x} QDs were observed with a good photothermal stability after irradiation for five cycles of heating and natural cooling. This excellent photothermal effect raised from the MoO_{3-x} QDs is retained in the PDMS matrix as in aqueous solution. The addition of 4%, 6%, 8% 10% of MoO₃x QDs was added into the PDMS solution to fabricate bioinspired surfaces

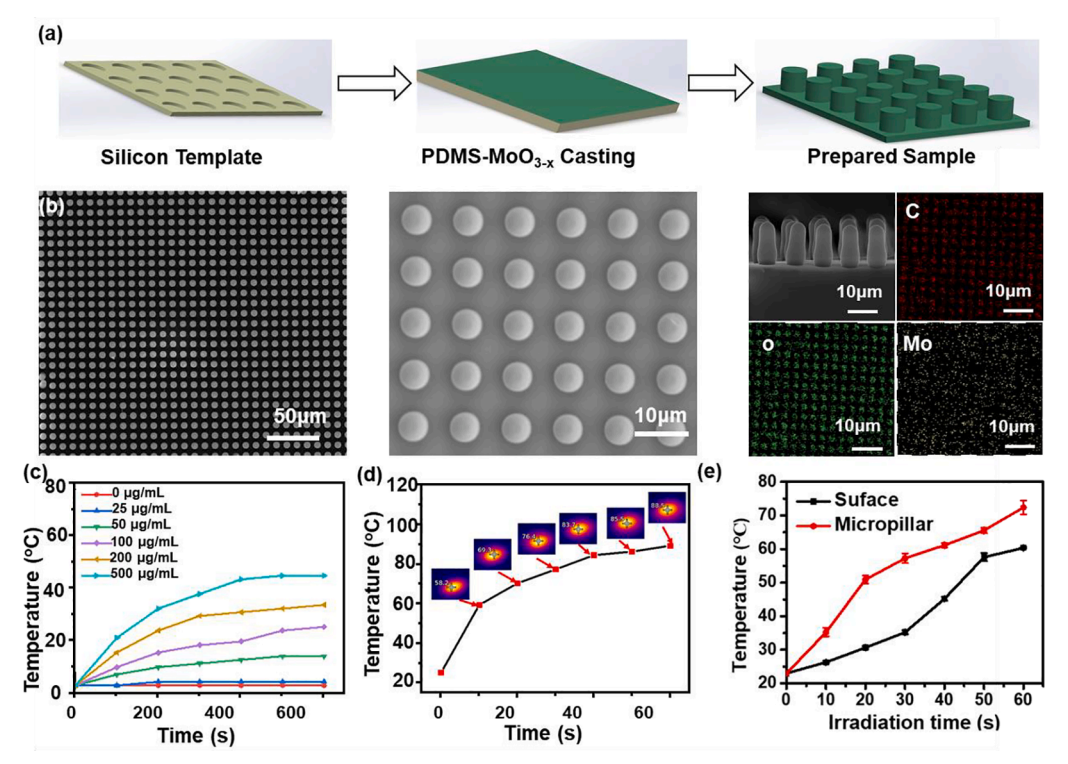


Fig. 3. (a) Schematics of the preparation of adhesive surface. (b) From left to right are top-view SEM image of the sample surface; zoomed-in top-view SEM image; SEM image of the sample surface from side view; and EDX mapping shows the elements of O, C, and Mo from left to right; (c) Temperature change of MoO3-x solution with different concentrations under 808 nm laser irradiation for 10 min; (d) Infrared thermal image and the temperature of the MoO₃. x-PDMS adhesive surface under 808 nm laser irradiation for 60 s, the of molecular mechanism of the MoO3-x QDs and PDMS matrix in the micropillar arrays was appeared in the illustration. (e) Temperature changes of planar and micropillar array PDMS-MoO_{3-x} under laser irradiation.

was tested under the irradiation of 808 nm near infrared (NIR) light. Thermal imaging cameras are used to record real-time temperature changes of the sample during the NIR irradiation. As shown in Fig. 3d, the temperature of 10% MoO_{3-x} -PDMS adhesive surface had risen to 88.5 °C from room temperature within 1 min, and the heating effect is

better than that of MoO_{3-x} solution at the same concentration. The corresponding infrared thermal images of Fig. S12a, 12b and 12c show the maximum temperature that can be reached by the biomimetic surface with 4%, 6% and 8% MoO_{3-x} concentration under the same conditions. Similarly, the photothermal effect could be regulated by

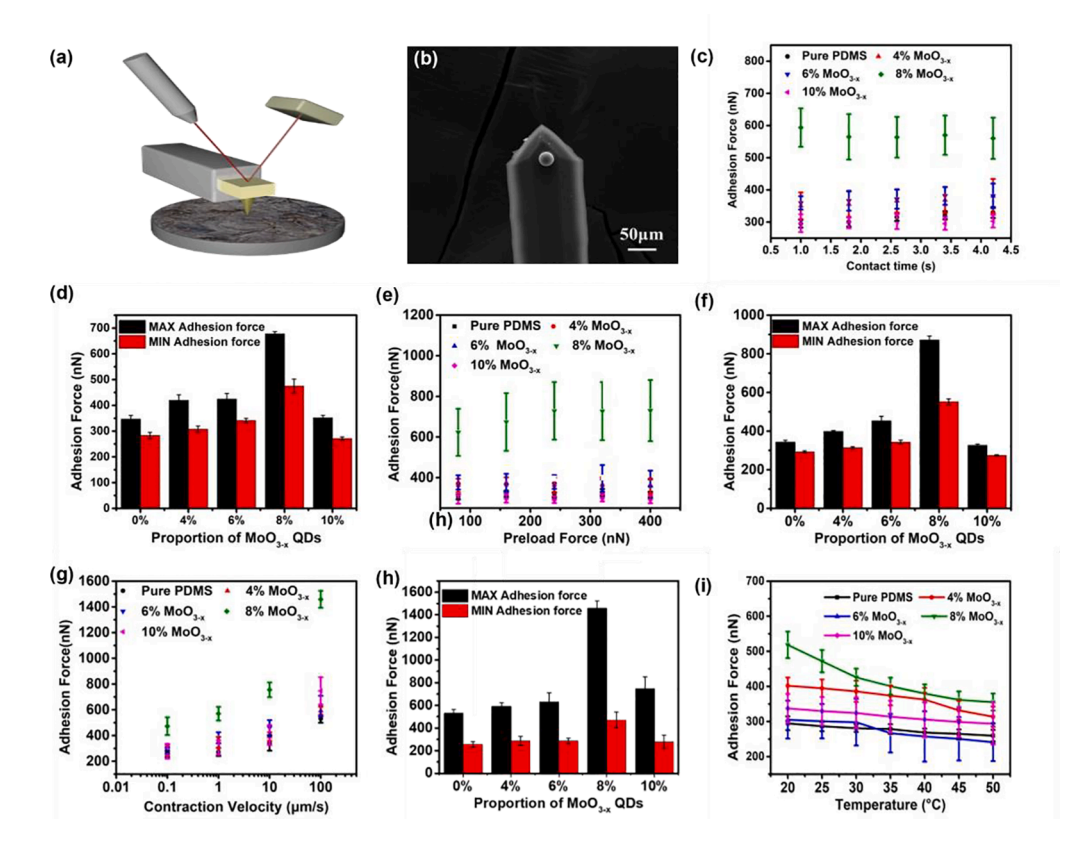


Fig. 4. (a) Schematic of the principle of AFM; (b) SEM images of a PS microparticle (diameter: 5.296 µm) glued on a tip-less AFM cantilever; Adhesion performance of the bioinspired micropillar under different factors: (c) contact time; (d) maximum and minimum adhesion force for the contact time changes in (c); (e) preload force; (f) maximum and minimum adhesion force for the preload force changes in (e); (g) retraction velocity; and (h) maximum and minimum adhesion force the retraction velocity changes in (g). (i) Influence of temperature on adhesion force of PDMS - MoO_{3-x} single micropillar.

changing the concentration of MoO_{3-x} QDs in the initial mixture. We further explore the influence of the micropillar structure of MoO_{3-x} -PDMS surface on the photothermal effect. The Fig. S12d is the MoO_{3-x} -PDMS without a pillar structure and the Fig. S12e has an integral pillar structure. Differences in adhesion surface were observed with NIR irradiation when irradiated for 40 s. The heat collection effect of the pillar structure was significantly greater than that of the planar structure. (Fig. 3e) It can be concluded that the temperature increase of the MoO_{3-x} -PDMS surface is a synergistic effect of a pillar structure and MoO_{3-x} concentration. The prepared MoO_{3-x} QDs not only have excellent photothermal properties, but this performance is retained in the bionic surface and show better effects.

2.3. Key factors influencing adhesive properties of the MoO_{3-x} -PDMS bioinspired surfaces

This section is mainly focused on adhesive properties of the bioinspired surfaces under the different conditions. The adhesion of the MoO_{3-x}-PDMS surface was measured by the Atomic Force Microscope (AFM) and the test setup is shown in Fig. 4a. A modified probe was obtained by bonding a Polystyrene (PS) nanoparticle to the free end of a tipless AFM cantilever as shown in Fig. 4b. The adhesive force between the PS modified probe and the bio-inspired surface can be determined by obtaining the entire force curve from complete separation to real compressive contact (the approaching stage), and from real compressive contact to full separation (the retracting stage), where a fixed level of compressive preloading can be setup for each scenario. We discover that when the mixing ratios of the MoO_{3-x} QDs are 8%, the adhesion force of the surface is the largest. Meanwhile, to delineate the key factors influencing the adhesion properties of the bioinspired surfaces, the dry adhesion between the adhesion surface and the tip of the nanosphere modified atomic force microscope was tested under various conditions including the contact times, preload force and retraction speed. Fig. 4c and 4d show the relationship between the contact time of the AFM tip and the bioinspired surface, where the contact time changed from 1.0 to 4.5 s, and the adhesion force of the MoO_{3-x}-PDMS surface remains relatively stable. Similarly, the relationship between preloading force and adhesion force are shown in Fig. 4e and 4f. With the preloading force increased from 80 to 400 nN, the final adhesion of samples changed to 3.61% -0.82%, 4.90%, 17.10%, -0.09% from their initial adhesion, respectively. Since the preload force and contact time will not cause chemical changes inside or on the surface of the sample, these two factors have no significant effect on the adhesion of the bioinspired surface. As shown in Fig. 4g and 4 h, when the contact time and load force are maintained at 3 s and 100 nN, four retraction speeds (0.1, 1, 10 and 100 µm/s) are used to study the speed's effect on the adhesion. The adhesion of samples is increased by 106.65%, 120.00%, 208.80%, 168.95% when compared to their initial adhesion. The the adhesion force increases rapidly with increasing the contraction velocity. This phenomenon is consistent with the dynamic model we have established in the past [29]. Meanwhile, the results of the measurements demonstrate the samples have the maximum adhesion force when the content of the MoO_{3-x} QDs is 8%, which corresponds to the previous experimental results. In the above experiments, the temperature of the biomimetic surface will increase significantly under the irradiation of infrared laser. Exploring the dependence of the adhesion of the material with the temperature change will be beneficial to the further application of the material. As shown in Fig. 4i, when the temperature is increased from 20 $^{\circ}\text{C}$ to 50 $^{\circ}\text{C},$ the adhesion forces of all the samples decrease significantly, indicating the negative influence of increased temperature on the adhesion. Therefore, we speculate that when the surface temperature of MoO_{3-x}-PDMS micropillar is increased by laser irradiation, its adhesion performance will also decrease at the same time. This property also provides the basis for the remote infrared control and controllable adhesion of the bioinspired surface.

2.4. The application of the MoO_{3,x}-PDMS bio-inspired micropillar arrays.

The MoO_{3-x}-PDMS bioinspired surface exhibits excellent adhesion due to its hierarchical array structure, which could be applied in the gripper of modern machines in a simple way to increase the mechanical endurance. In the gripping experiment, we installed the PDMS and MoO_{3-x}-PDMS columnar structure surfaces on the bendable bionic grippers for comparative experiments. (Fig. 5a,) The gripper fixed it on the bracket to make it parallel to each other, and passed the upper pipe to inflate to make it bend and deform to better simulate the state when the wrist is grasped. (Movie S1-S3) Then it was loaded with a certain mass of weight on the smooth glass surface cube with thin lines, and the weight was loaded until the glass cubes fell off. The ultimate loadbearing capacity of a gripper with MoO_{3-x}-PDMS surface (Fig. 5a(i)) is 0.25 kg more than PDMS surface (Fig. 5a(ii)). In addition to the good adhesion performance of this bionic surface under normal conditions, its unique photothermal response changes in adhesion also provide the possibility for its further application. As shown in Fig. 5b, we show the photothermal response mechanism of the inside of the bionic surface and the surface in contact with the glass interface. The molecular mechanism between the MoO_{3-x} QDs and the PDMS matrix in the micropillar arrays illustrates the internal changes of the bionic surface. We conducted Fourier transform infrared absorption (FTIR) tests on the $MoO_{3\text{-x}}\text{-PDMS}$ surface at 20 $^{\circ}\text{C}$ and 70 $^{\circ}\text{C}$. The test results show that the intensity of the strong absorption peak at 3280 cm⁻¹ increases (Fig. S13), indicating that the concentration of hydrogen bonds in the MoO_{3-x}-PDMS molecule increases after the temperature rises. The increase of intramolecular hydrogen bonds reduces the formation position of the hydrogen bond force between the surface of the biomimetic material and the glass or PS microspheres [30,31], resulting in a decrease in adhesion. At the same time, as the internal temperature of the MoO_{3-x}-PDMS surface rises, the temperature gradient formed in the inside and outside directions of the adhesive sample causes the expansion and bending of the overall structure, so that the contact area with the glass surface becomes smaller and the contact surface finally falls off. The Finite Element Analysis (FEA) simulation shows a snapshot of the selfexfoliation process caused by the temperature gradient, which proves the self-exfoliation caused by the temperature gradient (Fig. S14). As shown in Fig. S15, the adhesive surface was obviously bent after 60 s of laser irradiation. The test results of the shear force after laser irradiation for different times indicated that the shear adhesion force assumed a decreasing trend as the irradiation time increased as well (Fig. S18). The repeated adhesive switching on-and-off experiments can find that the surface has good reversible adhesion stability. (Fig. S19) Remote control of the state of adhesion of the MoO3-x-PDMS bioinspired micropillar arrays can be realized using infrared laser. As shown in Fig. 5c, after the MoO_{3-x}-PDMS is properly attached to a transparent beaker filled with 200 ml water, it can hold the beaker's entire weight. Then, after irradiating the contact area with an infrared laser, the MoO_{3-x}-PDMS surface bends, causing the initial contact area to become smaller and the loadbearing capacity to decrease, so the beaker will slide down and fall. Therefore, thermal and adhesive progression of the MoO_{3-x}-PDMS surface via NIR laser irradiation facilitated the adjustability of adhesion and release, indicating their potential as remote switching adhesives.

3. Conclusions

In this work, we successfully obtained MoO_{3-x} QDs with excellent photothermal property, and second applied them into the geckoinspired micropillar array to achieve a photo-controllable adhesive surface. This novel adhesive is composed of the MoO_{3-x} QDs as the functional ingredient and PDMS as the matrix of the micropillar arrays. When the temperature of the MoO_{3-x} -PDMS surface was increased from 20 °C to 88.5 °C by NIR exposure, the adhesion force can be reduced by 40%. This photothermal property stems from the oxygen vacancy formed in MoO_{3-x} , which enables the QDs to adsorb the ultra-red

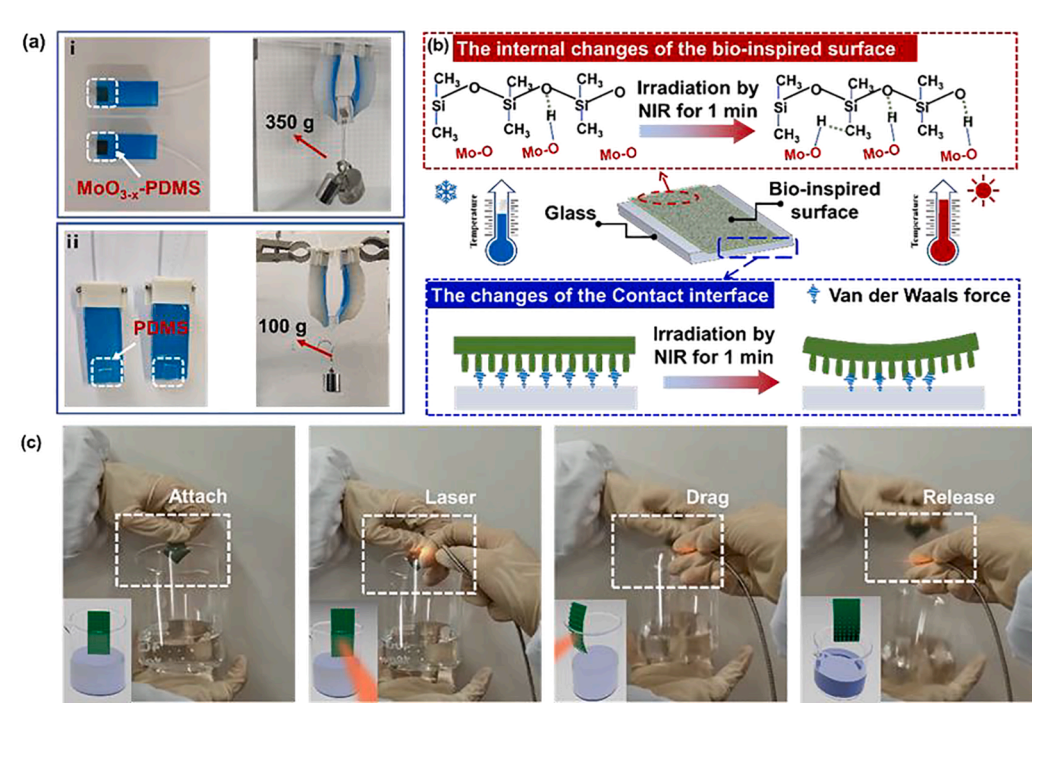


Fig. 5. (a) i. The soft robotic grippers with $\mathrm{MoO}_{3\text{-x}}\text{-PDMS}$ micropillar structure grab the weight with a maximum weight of 0.35 kg; ii. T The soft robotic grippers with PDMS micropillar structure grab the weight with a maximum weight of 0.1 kg; (b) Schematic diagram of the internal microstructure of the laser-triggered bionic surface temperature change and the contact with the macroscopic surface; (c) Experimental demonstration of photo-detachable bioinspired adhesive. (Inset: schematics of the photo-detachable mechanism).

spectrum with a lower energy to generate large amount of heat. The temperature increase causes the micropillars to bend away from each other to reduce the contact points with the target surface and peel off. Meanwhile, we have designed a gripper to successfully grab heavy objects of up to 3.6 N. These discoveries make it possible to create the next generation of photo-controllable, gecko-inspired surfaces, micro-/nano manipulators/selectors and other versatile, responsive smart materials and structures, applicable in advance manufacturing, aerospace, biomedical and energy related fields.

4. Experimental

4.1. Preparation of MoO_{3-x} QDs

An aqueous solution (10 ml) with 30% ethanol content was prepared and 50 mg of MoS_2 powder was dispersed into the 10 ml solution. Then the mixed solution was sonicated for 2 h to achieve good dispersity. The 8.5 ml prepared solution and 1.5 ml 30% H_2O_2 were mixed together, and then quickly transferred to the supercritical CO_2 apparatus, which was composed of a stainless-steel autoclave with a temperature controller and a heating jacket. The autoclave was heated to 60 °C and gradually injected with CO_2 until the pressure went up to 40 MPa. Then the CO_2 was released gradually at a placid speed after 3 h. Subsequently, the reacted solution was put into the centrifuge and ran at 6000 rpm for 15 min in order to remove the aggregates. The supernatant was taken as the QDs solution prepared.

4.2. Preparation of the MoO_{3-x} -PDMS micropillar arrays

PDMS was mixed with a curing agent (Sylgard 184) at a ratio of 10:1. MoO_{3-x} QDs (4, 6, 8, 10 % weight percentage) was added into the PDMS mixture before curing. Then, the mixture was put into a vacuum pump to degas. About 3 ml of trimethyl siloxane was dropped onto the silicon template for 30 min (to facilitate final debonding). After that, the mixed solution of PDMS and QDs (PDMS - QDs) was poured on the silicon template and then cured in the oven at a temperature of 60 °C for 9 h.

4.3. Characterization

The Zeiss Sigma 500 and Bruker XFlash 6/30 were used to capture the scanning electron microscope (SEM) and energy-dispersive X-ray spectroscopy (EDX) images of the sample. A Dimension Icon AFM was used to measure the adhesion force on individual micropillars. The photothermal effect of the samples were recorded with an Infrared Thermal Imager (Testo 865) under the NIR laser light (808 nm). XANES and near edge X-ray absorption fine structure (NEXAFS) spectra experiments were performed at the photoemission end-station at beamline BL10B in the National Synchrotron Radiation Laboratory (NSRL) in Hefei, China.

4.4. Preparation of the AFM probes with single seta/spatula or PS microparticle

PS micro-particles (250 mg/10 ml) were purchased from Great goose technology Co. LTD (Tianjin, China). The PS particle probes were prepared with the same procedure similar to how the single seta was bonded. Every probe was examined before and after the AFM test using a scanning electron microscope (SEM, FEI Inc.), to exclude premature failures due to poor bonding and/or excessive glue.

4.5. Simulation

Density functional theory (DFT) calculations were performed using the Vienna ab initio simulation package (VASP). The project-augmented wave (PAW) pseudopotentials and Perdew–Burke–Ernzerhof (PBE) exchange–correlation functional was employed. Spin-polarization was considered in all calculations. Van der Waal forces were incorporated using the DFT-D3 method. Wavefunctions were expanded using a planewave basis set with a kinetic energy cut off of 500 eV and the geometries were fully relaxed until the residual force convergence value on each atom became less than 0.02 eV/Å-1. In optimizing the structure, we chose $7 \times 2 \times 7$ and $1 \times 1 \times 1$ K-point mesh for the bulk structure (Fig. S16a) and the quantum dot structure (Fig. S16b). In the calculations of the electronic structure, we chose $15 \times 4 \times 15$ and $3 \times 3 \times 3$ K-point mesh for the bulk structure and the quantum dot structure. There are three types of models that were built: bulk phases, QDs, and QDs

with oxygen vacancies. For the bulk phase, we used $1 \times 3 \times 1$ -unit cells as shown in Fig. S17a. For the QDs, we constructed a structure with about 10 Å in the a and c directions and a single layer in the b direction as shown in Fig. S17b. Vacuum layers above 10 Å were added in the a, b, and c directions to eliminate the interaction between periodic boundary conditions. The H atom is used to saturate the O atom on the edge. For oxygen vacancies, two types of edge oxygen vacancies and two types of internal oxygen vacancies are considered as shown in Fig. S17c-f.

Declaration of Competing Interest

The authors declare that they have no known competing financial interests or personal relationships that could have appeared to influence the work reported in this paper.

Acknowledgements

This work was supported by National Nature Science Foundation of China (grant numbers 51875577), Tribology Science Fund of State Key Laboratory of Tribology (grant numbers SKLTKF16A06). T.S.H. acknowledges the support from the U.S. National Science Foundation (Award No. 2004251).

Appendix A. Supplementary data

Supplementary data to this article can be found online at https://doi.org/10.1016/j.cej.2021.134081.

References

- [1] X. Dong, H. Zhao, J. Li, Y. Tian, H. Zeng, M.A. Ramos, T.S. Hu, Q. Xu, Progress in Bioinspired Dry and Wet Gradient Materials from Design Principles to Engineering Applications, iScience 23 (2020) 101749.
- [2] K. Autumn, Y.A. Liang, S.T. Hsieh, W. Zesch, W.P. Chan, T.W. Kenny, R. Fearing, R. J. Full, Adhesive Force of a Single Gecko Foot-Hair, Nature 405 (6787) (2000) 691 695
- [3] S. Hu, S. Lopez, P.H. Niewiarowski, Z. Xia, Dynamic self-cleaning in gecko setae via digital hyperextension, J. Royal Soc., Interface / the Royal Society 9 (76) (2012) 2781–2790
- [4] Y. Tian, N. Pesika, H. Zeng, K. Rosenberg, B. Zhao, P. McGuiggan, K. Autumn, J. Israelachvili, Adhesion and friction in gecko toe attachment and detachment, Proc. Natl. Acad. Sci. 103 (2006) 19320.
- [5] H. Shahsavan, S.M. Salili, A. Jákli, B. Zhao, Thermally Active Liquid Crystal Network Gripper Mimicking the Self-Peeling of Gecko Toe Pads, Adv. Mater. 29 (2017) 1604021
- [6] Y. Zhang, S. Ma, B. Li, B. Yu, H. Lee, M. Cai, S.N. Gorb, F. Zhou, W. Liu, Gecko's Feet-Inspired Self-Peeling Switchable Dry/Wet Adhesive, Chem. Mater. 33 (8) (2021) 2785–2795
- [7] D.i. Tan, X. Wang, Q. Liu, K. Shi, B. Yang, S. Liu, Z.-S. Wu, L. Xue, Switchable Adhesion of Micropillar Adhesive on Rough Surfaces, Small 15 (50) (2019) 1904248, https://doi.org/10.1002/smll.v15.5010.1002/smll.201904248.
- [8] S. Song, D.-M. Drotlef, C. Majidi, M. Sitti, Controllable load sharing for soft adhesive interfaces on three-dimensional surfaces, Proc. Natl. Acad. Sci. 114 (22) (2017) E4344–E4353.
- [9] S. Li, H. Liu, H. Tian, C. Wang, D. Wang, Y. Wu, J. Shao, Dytiscus lapponicus-Inspired Structure with High Adhesion in Dry and Underwater Environments, ACS Appl. Mater. Interfaces 13 (35) (2021) 42287–42296.

- [10] S. Li, H. Tian, J. Shao, H. Liu, D. Wang, W. Zhang, Switchable Adhesion for Nonflat Surfaces Mimicking Geckos' Adhesive Structures and Toe Muscles, ACS Appl. Mater. Interfaces 12 (35) (2020) 39745–39755.
- [11] Y. Ma, S. Ma, Y. Wu, X. Pei, S.N. Gorb, Z. Wang, W. Liu, F. Zhou, Adhesives: Remote Control over Underwater Dynamic Attachment/Detachment and Locomotion (Adv. Mater. 30/2018), Advanced Materials 30 (2018) 1870222.
- [12] K.e. Ni, Q.i. Peng, E. Gao, K. Wang, Q. Shao, H. Huang, L. Xue, Z. Wang, Core-Shell Magnetic Micropillars for Reprogrammable Actuation, ACS Nano 15 (3) (2021) 4747–4758
- [13] D.-M. Drotlef, P. Blümler, A. del Campo, Magnetically Actuated Patterns for Bioinspired Reversible Adhesion (Dry and Wet), Adv. Mater. 26 (2014) 775–779.
- [14] Y. Lin, Z. Hu, M. Zhang, T. Xu, S. Feng, L. Jiang, Y. Zheng, Magnetically Induced Low Adhesive Direction of Nano/Micropillar Arrays for Microdroplet Transport, Adv. Funct. Mater. 28 (2018) 1800163.
- [15] B. Dai, S. Li, T. Xu, Y. Wang, F. Zhang, Z. Gu, S. Wang, Artificial Asymmetric Cilia Array of Dielectric Elastomer for Cargo Transportation, ACS Appl. Mater. Interfaces 10 (49) (2018) 42979–42984.
- [16] H. Tian, H. Liu, J. Shao, S. Li, X. Li, X. Chen, An electrically active gecko-effect soft gripper under a low voltage by mimicking gecko's adhesive structures and toe muscles, Soft Matter 16 (24) (2020) 5599–5608.
- [17] D.-J. Guo, R. Liu, Y.u. Cheng, H. Zhang, L.-M. Zhou, S.-M. Fang, W.H. Elliott, W. Tan, Reverse adhesion of a gecko-inspired synthetic adhesive switched by an ion-exchange polymer-metal composite actuator, ACS Appl. Mater. Interfaces 7 (9) (2015) 5480–5487.
- [18] Z. Ye, G.Z. Lum, S. Song, S. Rich, M. Sitti, Phase Change of Gallium Enables Highly Reversible and Switchable Adhesion, Adv. Mater. 28 (25) (2016) 5088–5092.
- [19] M. Frensemeier, J.S. Kaiser, C.P. Frick, A.S. Schneider, E. Arzt, R.S. Fertig, E. Kroner, Temperature-Induced Switchable Adhesion using Nickel-Titanium-Polydimethylsiloxane Hybrid Surfaces, Adv. Funct. Mater. 25 (20) (2015) 3013–3021.
- [20] H. Cho, G. Wu, J. Christopher Jolly, N. Fortoul, Z. He, Y. Gao, A. Jagota, S. Yang, Intrinsically reversible superglues via shape adaptation inspired by snail epiphragm, Proc. Natl. Acad. Sci. 116 (2019) 13774.
- [21] S. Saito, S. Nobusue, E. Tsuzaka, C. Yuan, C. Mori, M. Hara, T. Seki, C. Camacho, S. Irle, S. Yamaguchi, Light-melt adhesive based on dynamic carbon frameworks in a columnar liquid-crystal phase, Nat. Commun. 7 (2016) 12094.
- [22] Y. Zhou, M. Chen, Q. Ban, Z. Zhang, S. Shuang, K. Koynov, H.-J. Butt, J. Kong, S. i. Wu, Light-Switchable Polymer Adhesive Based on Photoinduced Reversible Solid-to-Liquid Transitions, ACS Macro Lett. 8 (8) (2019) 968–972.
- [23] X. Wang, D.i. Tan, S. Hu, Q. Li, B. Yang, Z. Shi, R. Das, X. Xu, Z.-S. Wu, L. Xue, Reversible Adhesion via Light-Regulated Conformations of Rubber Chains, ACS Appl Mater Interfaces 11 (49) (2019) 46337–46343.
- [24] L.F. Boesel, C. Greiner, E. Arzt, A. del Campo, Gecko-Inspired Surfaces: A Path to Strong and Reversible Dry Adhesives, Adv. Mater. 22 (2010) 2125–2137.
- [25] D. Ding, W. Guo, C. Guo, J. Sun, N. Zheng, F. Wang, M. Yan, S. Liu, MoO3–x quantum dots for photoacoustic imaging guided photothermal/photodynamic cancer treatment, Nanoscale 9 (5) (2017) 2020–2029.
- [26] E. Kizilkan, J. Strueben, A. Staubitz, S.N. Gorb, Bioinspired photocontrollable microstructured transport device, Sci. Rob. 2 (2) (2017), https://doi.org/10.1126/ scirobotics.aak9454.
- [27] Q. Tian, F. Jiang, R. Zou, Q. Liu, Z. Chen, M. Zhu, S. Yang, J. Wang, J. Wang, J. Hu, Hydrophilic Cu9S5 Nanocrystals: A Photothermal Agent with a 25.7% Heat Conversion Efficiency for Photothermal Ablation of Cancer Cells in Vivo, ACS Nano 5 (2011) 9761–9771.
- [28] G. Song, J. Shen, F. Jiang, R. Hu, W. Li, L. An, R. Zou, Z. Chen, Z. Qin, J. Hu, Hydrophilic Molybdenum Oxide Nanomaterials with Controlled Morphology and Strong Plasmonic Absorption for Photothermal Ablation of Cancer Cells, ACS Appl. Mater. Interfaces 6 (6) (2014) 3915–3922.
- [29] Q. Xu, M. Li, L. Zhang, J. Niu, Z. Xia, Dynamic Adhesion Forces between Microparticles and Substrates in Water, Langmuir 30 (37) (2014) 11103–11109.
- [30] W. Song, Adhesion switch on a gecko-foot inspired smart nanocupule surface, Nanoscale 6 (22) (2014) 13435–13439.
- [31] M. Li, Q. Xu, X.u. Wu, W. Li, W. Lan, L. Heng, J. Street, Z. Xia, Tough Reversible Adhesion Properties of a Dry Self-Cleaning Biomimetic Surface, ACS Appl. Mater. Interfaces 10 (31) (2018) 26787–26794.